Quantitative Analyses of Hepatic OATP-Mediated Interactions Between Statins and Inhibitors Using PBPK Modeling With a Parameter Optimization Method

T Yoshikado[1], K Yoshida[2], N Kotani[3], T Nakada[4], R Asaumi[5], K Toshimoto[1], K Maeda[2], H Kusuhara[2] and Y Sugiyama[1]

This study aimed to construct a widely applicable method for quantitative analyses of drug–drug interactions (DDIs) caused by the inhibition of hepatic organic anion transporting polypeptides (OATPs) using physiologically based pharmacokinetic (PBPK) modeling. Models were constructed for pitavastatin, fluvastatin, and pravastatin as substrates and cyclosporin A (CsA) and rifampicin (RIF) as inhibitors, where enterohepatic circulations (EHC) of statins were incorporated. By fitting to clinical data, parameters that described absorption, hepatic elimination, and EHC processes were optimized, and the extent of these DDIs was explained satisfactorily. Similar *in vivo* inhibition constant (K_i) values of each inhibitor against OATPs were obtained, regardless of the substrates. Estimated K_i values of CsA were comparable to reported *in vitro* values with the preincubation of CsA, while those of RIF were smaller than reported *in vitro* values (coincubation). In conclusion, this study proposes a method to optimize *in vivo* PBPK parameters in hepatic uptake transporter-mediated DDIs.

Study Highlights

WHAT IS THE CURRENT KNOWLEDGE ON THE TOPIC?

☑ Clinically relevant examples of transporter-mediated drug–drug interactions (tDDIs) have been reported. *In vitro–in vivo* discrepancies exist in the prediction of tDDIs, which may hamper the practical use of physiologically based pharmacokinetic (PBPK) modeling.

WHAT QUESTION DID THIS STUDY ADDRESS?

☑ This study aimed to propose a method to construct a feasible PBPK modeling to determine *in vivo* parameters in clinical DDIs that are primarily caused by the inhibition of hepatic organic anion transporting polypeptides (OATPs).

WHAT THIS STUDY ADDS TO OUR KNOWLEDGE

☑ PBPK model parameters that adequately reproduced the magnitudes of DDIs between statins and OATP inhibitors were obtained. Similar *in vivo* inhibition constants (K_i) of cyclosporin A (CsA) against OATPs were obtained regardless of the substrates, which was explained by the reported *in vitro* K_i obtained after preincubation with CsA.

HOW THIS MIGHT CHANGE CLINICAL PHARMACOLOGY OR TRANSLATIONAL SCIENCE

☑ The *in vivo* parameter-optimization approach taken in this study might contribute to improving *in vitro–in vivo* extrapolation methods and establishing a methodology for the prediction of complex DDIs involving multiple processes.

Because combinations of multiple drugs are administered to patients in normal clinical situations, the prediction of drug–drug interaction (DDI) potential is essential for the appropriate clinical use of drugs with minimization of unfavorable side effects. For example, cerivastatin, which is one of the 3-hydroxy-3-methylglutaryl coenzyme A (HMG-CoA) reductase inhibitors, has been withdrawn from the market because of its association with lethal rhabdomyolysis, and recent reports suggest that the coadministration of gemfibrozil increases the risk of this side effect.[1,2] From the viewpoint of pharmacokinetics, gemfibrozil glucuronide greatly increases the plasma concentration of cerivastatin, which leads to increased exposure of cerivastatin to muscle tissues because of the mechanism-based inhibition of cytochrome P450 2C8 (CYP2C8)-mediated metabolism and the inhibition of the organic anion transporting polypeptide (OATP)-mediated hepatic uptake of cerivastatin.[3,4]

Thus, regulatory authorities ask sponsors to evaluate the potential risk of DDIs of newly submitted drugs, as both victims and

[1]Sugiyama Laboratory, RIKEN Innovation Center, RIKEN, Yokohama, Kanagawa, Japan; [2]Laboratory of Molecular Pharmacokinetics, Graduate School of Pharmaceutical Sciences, University of Tokyo, Tokyo, Japan; [3]Clinical Pharmacology Strategy Group, Translational Clinical Research Science & Strategy Dept., Chugai Pharmaceutical Co., Tokyo, Japan; [4]DMPK Research Laboratories Sohyaku, Innovative Research Division, Mitsubishi Tanabe Pharma, Chiba, Japan; [5]Pharmacokinetic Research Laboratories, Ono Pharmaceutical Co., Ibaraki, Japan. Correspondence: Y Sugiyama (ychi.sugiyama@riken.jp)

Received 21 January 2016; accepted 3 May 2016; advance online publication 12 May 2016. doi:10.1002/cpt.391

perpetrators. Based on the regulatory guidance/guidelines on DDIs, if the DDI risk is expected to be positive from simple "static model" analyses, clinical DDI studies using probe substrates/inhibitors are recommended. In this model, DDI risk is evaluated assuming that the theoretical maximum concentration of an inhibitor drug at the target site is maintained over time, to avoid false-negative prediction. This is suitable in the early phase of drug development, as detailed clinical pharmacokinetic parameters of new drug candidates are not available at this stage.[5,6] However, in principle this model overestimates the magnitude of DDIs, which often leads to false-positive predictions. In addition, this method depends on inhibition constants (K_i) mostly evaluated *in vitro*, which might be affected by experimental conditions (i.e., coincubation or preincubation with cyclosporin A (CsA)).[7,8]

Conversely, to accurately predict the change in the blood and tissue concentration of victim drugs caused by DDIs, a physiologically based pharmacokinetic (PBPK) model that considers the time-dependent change in the inhibitor concentration can provide the time profiles of the plasma and tissue concentrations of a victim drug. When taking such a "dynamic model" approach, it is critical to set up various optimum PK parameters for both substrates and inhibitors. Several quantitative analyses of metabolism-mediated DDIs (mDDIs) involving the inhibition and/or induction of metabolic enzymes using PBPK models have been reported.[9,10] Regarding transporter-mediated DDIs (tDDIs), the number of clinically relevant examples has been increasing rapidly. The inhibition of hepatic OATPs (OATP1B1 and OATP1B3) is among the important tDDI mechanisms. The systemic exposure of various statins (OATP substrates) was significantly increased by the concomitant administration of OATP inhibitors, such as CsA, rifampicin (RIF), and gemfibrozil.[5,6,11] Moreover, recent reports provided quantitative predictions for OATP-mediated DDIs between statins and CsA/RIF/gemfibrozil[12–14] based on PBPK models. In the process of their analyses, those authors suggested some *in vitro–in vivo* discrepancies in PK parameters, especially regarding hepatic intrinsic clearances (uptake, efflux from hepatocytes into the blood, biliary excretion, and metabolism) based on the extended clearance concept,[15] and K_i values for OATPs. Such discrepancies may hamper the practical use of PBPK modeling for DDI prediction via a bottom-up approach, in which model parameters are determined by scaling up *in vitro* experimental results. Therefore, optimization of pharmacokinetic parameters of several drugs to account for the clinical data (collection of *in vivo* parameters) will improve the accuracy of a global *in vitro–in vivo* extrapolation (IVIVE) methodology.

Taking a top-down approach, the present study aimed to construct a widely applicable method for optimizing PBPK model parameters that adequately describe the clinically observed interactions between statins and CsA/RIF, which were primarily caused by the inhibition of hepatic OATPs. The concomitant administration of CsA caused 4.6-fold and 3.5-fold increases in the area under the plasma concentration–time curves (AUCs) of pitavastatin (PTV) and fluvastatin (FLV), respectively.[16,17] The concomitant administration of RIF caused 6.7-fold and 4.6-fold increases in the AUCs of PTV and pravastatin (PRV), respectively.[18,19] After constructing PBPK models, the *in vivo* PK parameters of statins and the *in vivo* K_i values by CsA/RIF were optimized via fitting to the blood concentration–time profiles in both control and DDI conditions, which might be useful for predicting other DDIs involving these drugs.

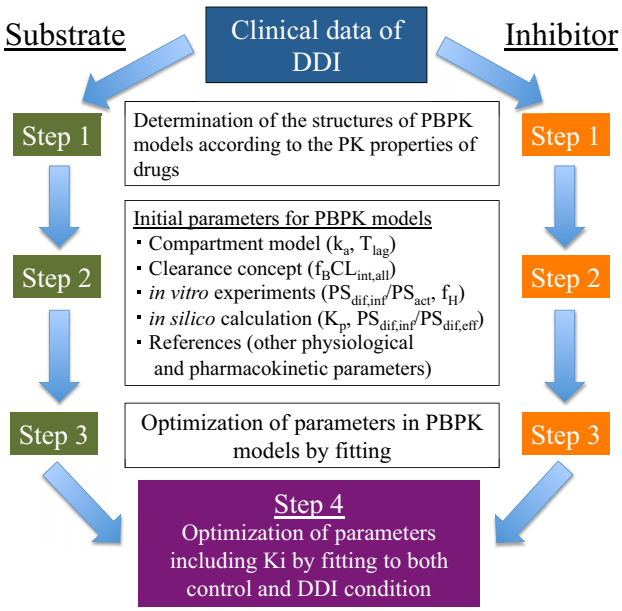

Figure 1 Scheme of the workflow of parameter optimization in the PBPK models to describe hepatic OATP-mediated DDIs. Step 1, Determination of the structures of PBPK models according to the PK properties of drugs; step 2, determination of initial parameters for PBPK models based on clinical information, *in vitro* data, and *in silico* calculation; step 3, optimization of PK parameters by fitting to the blood concentration–time profile after single administration of each drug; step 4, optimization of PK parameters of the substrate and the K_i value of the inhibitor for OATPs by simultaneous fitting to clinical PK data of the substrate without and with coadministration of the inhibitor. $CL_{int,all}$, hepatic overall intrinsic clearance; f_B, protein unbound fraction in blood; f_H, hepatic protein unbound fraction; k_a, absorption rate constant; K_p, tissue/blood concentration ratio; PS_{act}, active uptake intrinsic clearance on the sinusoidal membrane; $PS_{dif,eff}$, efflux intrinsic clearance by passive diffusion through sinusoidal membrane; $PS_{dif,inf}$, influx intrinsic clearance by passive diffusion through sinusoidal membrane; T_{lag}, lag time in intestinal absorption. [Color figure can be viewed at wileyonlinelibrary.com]

RESULTS

Workflow of the construction of PBPK models to reproduce the DDIs caused by the inhibition of hepatic OATPs

A top-down approach was taken to optimize PBPK model parameters for statins and CsA/RIF using clinical data for hepatic OATP-mediated DDIs, as described in the Methods (vs. CsA cases) and **Supplemental Text** (vs. RIF cases). **Figures 1** and **2** show the workflow of stepwise methods and structure of PBPK models, respectively. All initial and fixed parameters are summarized in **Table 1**, **Supplemental Tables 1 (A,B)**, **2 (A,B,E,F)**, and **3 (A,C,D,G,H,K,L)**. The sets of assumptions used in the PBPK models are described in **Supplemental Table 1 (C,D)**.

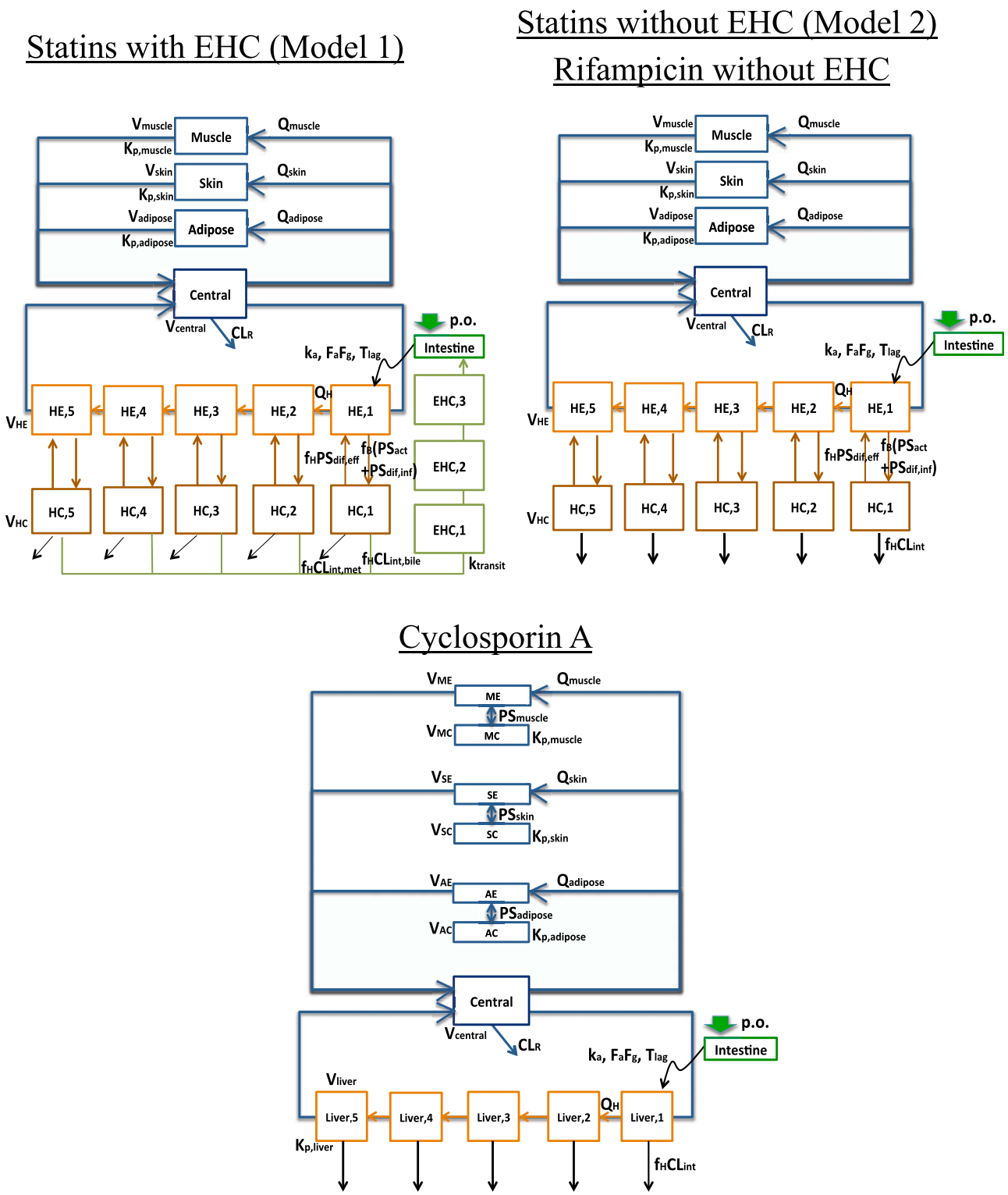

Figure 2 Structures of the PBPK models for describing the blood concentration–time profiles of statins, rifampicin, and cyclosporin A. The liver compartment was divided into five units of extrahepatic and hepatocytes compartments to mimic the dispersion model. EHC was incorporated in Model 1 of statins, but not in Model 2 of statins and the models of the inhibitors. Rapid equilibrium in the liver and slow permeability in muscle, skin, and adipose tissues were incorporated in the model of cyclosporin A. AC, adipose cells; AE, adipose extracellular space; $CL_{int,bile}$, intrinsic clearance of biliary excretion; $CL_{int,met}$, intrinsic clearance of hepatic metabolism; CL_R, renal clearance; F_aF_g, intestinal availability; f_B, protein unbound fraction in blood; f_H, hepatic protein unbound fraction; HC, hepatocytes; HE, hepatic extracellular space; k_a, absorption rate constant; K_p, tissue/blood concentration ratio; $k_{transit}$, transit rate constant for EHC; MC, muscle cells; ME, muscle extracellular space; PS_{act}, active uptake intrinsic clearance on sinusoidal membrane; $PS_{dif,inf}$, influx intrinsic clearance by passive diffusion through sinusoidal membrane; $PS_{dif,eff}$, efflux intrinsic clearance by passive diffusion through sinusoidal membrane; PS_{tissue}, permeability-surface area product in tissue; Q_{tissue}, blood flow rate in tissue; SC, skin cells; SE, skin extracellular space; T_{lag}, lag time in intestinal absorption; V_{tissue}, tissue volume. [Color figure can be viewed at wileyonlinelibrary.com]

Table 1 Initial parameters in pitavastatin/fluvastatin vs. cyclosporin A cases: PBPK models of cyclosporin A (A) and statins (B and C) with EHC (using R_{dif} values determined by *in vitro* experiments)

A. Initial parameters for cyclosporin A

k_a[a]	T_{lag}[a]	$K_{p,liver}$[b]	$f_H CL_{int}$[c]	PS_{muscle}[d]	PS_{skin}[d]	$PS_{adipose}$[d]	$K_{p,muscle}$[e]	$K_{p,skin}$[e]	$K_{p,adipose}$[e]
hr^{-1}	hr	—	L/hr	L/hr	L/hr	L/hr	—	—	—
0.91	0.30	11	1.69	517	78.9	21.5	0.51	2.34	2.97

B. Initial parameters for pitavastatin and inhibition constant ($K_{i,u}$) by cyclosporin A

	k_a[f]	T_{lag}[f]	$f_B CL_{int,all}$[g]	β[h]	R_{dif}[i]	γ[j]	f_{bile}[k]	$k_{transit}$[l]	$K_{i,u}$[m]
ID	hr^{-1}	hr	L/hr	(FIX)	(FIX)	(FIX)	—	hr^{-1}	μM
1	1.16	1.45	77.2	0.8	0.0345	0.244	0.60	1	0.0180
2	1.16	1.45	77.2	0.5	0.0345	0.244	0.60	1	0.0180
3	1.16	1.45	77.2	0.2	0.0345	0.244	0.60	1	0.0180

$\beta = CL_{int,all}/(PS_{act} + PS_{dif,inf})$, $R_{dif} = PS_{dif,inf}/PS_{act}$, $\gamma = PS_{dif,inf}/PS_{dif,eff}$

C. Initial parameters for fluvastatin and inhibition constant ($K_{i,u}$) by cyclosporin A

	k_a[f]	T_{lag}[f]	$f_B CL_{int,all}$[g]	β[h]	R_{dif}[i]	γ[j]	f_{bile}[k]	$k_{transit}$[l]	$K_{i,u}$[m]
ID	hr^{-1}	hr	L/hr	(FIX)	(FIX)	(FIX)	—	hr^{-1}	μM
1	1.08	0.50	113	0.8	0.173	0.243	0.16	1	0.0278
2	1.08	0.50	113	0.5	0.173	0.243	0.16	1	0.0278
3	1.08	0.50	113	0.2	0.173	0.243	0.16	1	0.0278

$\beta = CL_{int,all}/(PS_{act} + PS_{dif,inf})$, $R_{dif} = PS_{dif,inf}/PS_{act}$, $\gamma = PS_{dif,inf}/PS_{dif,eff}$

[a]Previously reported k_a and T_{lag} were used. [b]Set at $K_{p,liver}$ reported in rats. [c]Determined based on the clearance concept using reported i.v. data. [d]Permeability surface area product on tissue membranes (PS_{muscle}, PS_{skin}, and $PS_{adipose}$) determined in rats were multiplied by a common scaling factor (SF_{PS}). See detail in Methods. [e]*In silico* K_p values in the muscle, skin, and adipose tissues were multiplied by a common scaling factor (SF_{Kp}). See detail in Methods. [f]Determined by two-compartmental analyses to fit reported concentration–time profiles. As for pitavastatin, T_{lag} includes the delay of the coadministration after CsA (1 hr). [g]Calculated using Equations 9 and 11. [h]Fixed to three different values indicating different conditions of the major rate-determining processes in the hepatic intrinsic clearance. [i]Calculated according to Equations 2 and 6. [j]Calculation. See detail in Methods. [k]Calculated using Equation 12 and the pharmacokinetics data of statins in bile duct cannulated rats. [l]Set to 1 due to the lack of information. [m]Calculated using the observed AUCRs and I_{max} (Equation 13).

Fitting of the model for CsA to its blood concentration–time profile

The parameters for CsA in the PBPK model were obtained via fitting to its reported blood concentration–time profile[20] using initial parameters described in **Table 1A**. The blood concentration–time profile of orally administered CsA was reproduced, as shown in **Figure 3** (solid line), and parameters were optimized as shown in **Table 2A**; the K_p values in these tissues were 5.5-fold those calculated *in silico*, and permeability surface area-product (PS) values were 0.56-fold those originally estimated in rats. Using these parameters, an intrahepatic concentration–time profile was simulated, as shown in **Figure 3** (dotted line): the hepatic concentration of CsA was much higher than its blood concentration, which could be explained by the high $K_{p,liver}$ value. The parameters obtained for CsA were then used as fixed values in the next step.

Fitting of the models for statins to their blood concentration–time profiles under control and DDI conditions considering the inhibition of hepatic OATPs by CsA

The pharmacokinetic parameters in the PBPK model, including the enterohepatic circulations (EHC) of statins (EHC model), were optimized via simultaneous fitting to the blood concentration–time profiles of orally administered PTV or FLV[16,17] under both control and DDI conditions (Step 4), whereas the parameters obtained by single fitting to the control data (Step 3) did not reproduce the clinical data well (data not shown). First, based on a static model using the maximum blood concentration of CsA, initial $K_{i,u}$ values were estimated as described in the Methods; $K_{i,u}$ = 0.018 and 0.028 μM explained the 4.6-fold and 3.5-fold AUC increases observed in PTV vs. CsA and FLV vs. CsA, respectively. Subsequently, k_a, T_{lag}, $f_B CL_{int,all}$, f_{bile}, k_{bile}, and $K_{i,u}$ were set as free parameters, while hybrid parameters including R_{dif} (determined by *in vitro* experiments in this study), β, and γ values (see definitions in Methods) were fixed as described in **Table 1B,C**, and the model of each statin was fitted to the blood concentration–time profile to the same degree, regardless of the setting of β values (**Figure 4**). Among the parameters obtained that reproduced the clinical data (**Table 2B,C**), similar *in vivo* $K_{i,u}$ values of CsA were obtained for PTV (0.012 ± 0.002 μM) and for FLV (0.0096 ± 0.0042 μM). Conversely, the simulated intrahepatic concentrations of PTV (**Figure 4a–c**) and FLV (**Figure 4d–f**) varied depending on the setting of β values as 0.8, 0.5, or 0.2.

Fitting analyses were also performed using an *in vitro* R_{dif} value for PTV based on the data from three reports (a geometric mean

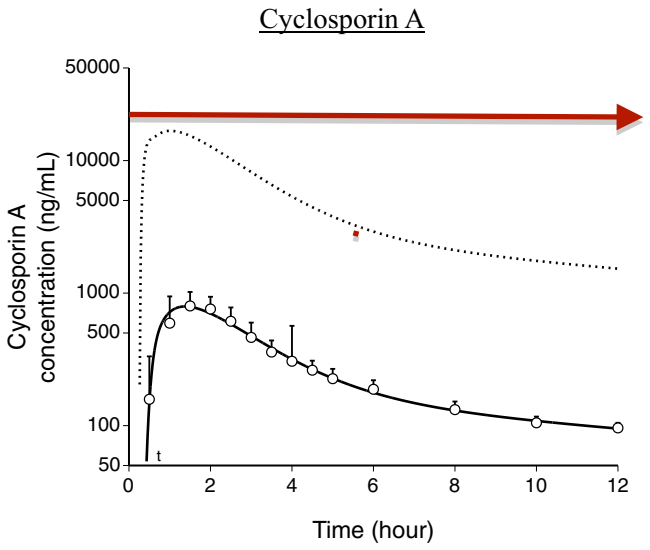

Figure 3 Fitted blood and liver concentration–time profile of CsA after the optimization of model parameters to explain PK data. The solid line represents a fitted blood concentration–time profile of orally administered CsA after parameter optimization in the PBPK model and the circles represent reported concentration–time profiles. The dotted line represents a simulated intrahepatic concentration–time profile (the first liver compartment in **Figure 2**). Optimized parameters are described in **Table 2A**.

value)[21–23] and that for FLV based on the data from one report[24] (**Suppl. Fig. 1, Suppl. Table 2A–D**). The *in vivo* $K_{i,u}$ values obtained were 0.0072 ± 0.0020 μM for PTV and 0.0041 ± 0.0035 μM for FLV, which were a little lower than those obtained by fitting analyses that were preformed using the *in vitro* R_{dif} values determined in this study (**Table 2B,C**).

Using PBPK models in which EHC was not taken into consideration (non-EHC model), a simultaneous fitting to the blood concentration–time profiles under both control and DDI conditions was performed (**Suppl. Fig. 2, Suppl. Table 2E–H**). However, the parameters obtained by fitting did not reproduce the clinical data, suggesting that the incorporation of EHC into the PBPK model for statins is necessary to describe accurately the blood concentration–time profiles of PTV and FLV.

Fitting of the models for statins to their blood concentration–time profiles under control and DDI conditions considering the inhibition of hepatic OATPs by RIF

Analyses of OATP-mediated DDI between PTV/PRV and RIF based on the parameter-optimization method were performed as described in detail in the **Supplemental Text**. Results are shown in **Supplemental Figures 3** and **4,** and **Supplemental Table 3**.

Table 2 Optimized parameters in pitavastatin/fluvastatin vs. cyclosporin A cases: PBPK models of cyclosporin A (A) and statins (B and C) with EHC (using R_{dif} values determined by *in vitro* experiments)

A. Optimized parameters for cyclosporin A

k_a	T_{lag}	$K_{p,liver}$	$f_H CL_{int}$	PS_{muscle} [a]	PS_{skin} [a]	$PS_{adipose}$ [a]	$K_{p,muscle}$ [b]	$K_{p,skin}$ [b]	$K_{p,adipose}$ [b]		
hr^{-1}	hr	—	L/hr	L/hr	L/hr	L/hr	—	—	—	SS	AIC
0.999 ± 0.353	0.254 ± 0.039	16.7 ± 4.0	0.587 ± 0.223	245 ± 26	37.4 ± 4.0	10.2 ± 1.1	2.98 ± 1.17	13.6 ± 5.3	17.3 ± 6.8	0.773	4.39

B. Optimized parameters for pitavastatin and inhibition constant ($K_{i,u}$) by cyclosporin A

	k_a	T_{lag}	$f_B CL_{int,all}$	β	R_{dif}	γ	f_{bile}	$k_{transit}$	$K_{i,u}$		
ID	hr^{-1}	hr	L/hr	(FIX)	(FIX)	(FIX)	—	hr^{-1}	μM	SS	AIC
1	1.06 ± 0.21	1.00 ± 0.42	51.5 ± 10.9	0.8	0.0345	0.244	0.330 ± 0.061	0.677 ± 0.101	0.0118 ± 0.0021	10.2	58.4
2	1.07 ± 0.21	1.00 ± 0.42	51.6 ± 10.8	0.5	0.0345	0.244	0.330 ± 0.060	0.679 ± 0.101	0.0118 ± 0.0020	10.2	58.5
3	1.08 ± 0.22	1.00 ± 0.41	51.9 ± 10.7	0.2	0.0345	0.244	0.332 ± 0.060	0.682 ± 0.101	0.0117 ± 0.0020	10.3	58.6

$\beta = CL_{int,all}/(PS_{act} + PS_{dif,inf})$, $R_{dif} = PS_{dif,inf}/PS_{act}$, $\gamma = PS_{dif,inf}/PS_{dif,eff}$. Values are shown as the mean ± standard deviation (SD).

C. Optimized parameters for fluvastatin and inhibition constant ($K_{i,u}$) by cyclosporin A

	k_a	T_{lag}	$f_B CL_{int,all}$	β	R_{dif}	γ	f_{bile}	$k_{transit}$	$K_{i,u}$		
ID	hr^{-1}	hr	L/hr	(FIX)	(FIX)	(FIX)	—	hr^{-1}	μM	SS	AIC
1	0.60 ± 0.16	0.39 ± 0.10	137.1 ± 18.5	0.8	0.173	0.243	0.654 ± 0.099	0.415 ± 0.093	0.00958 ± 0.00425	1.85	21.9
2	0.60 ± 0.16	0.39 ± 0.10	137.1 ± 18.4	0.5	0.173	0.243	0.654 ± 0.099	0.415 ± 0.093	0.00958 ± 0.00424	1.85	21.8
3	0.60 ± 0.16	0.39 ± 0.10	137.1 ± 18.3	0.2	0.173	0.243	0.654 ± 0.098	0.415 ± 0.092	0.00958 ± 0.00423	1.83	21.7

$\beta = CL_{int,all}/(PS_{act} + PS_{dif,inf})$, $R_{dif} = PS_{dif,inf}/PS_{act}$, $\gamma = PS_{dif,inf}/PS_{dif,eff}$. Values are shown as the mean ± standard deviation (SD).

Values are shown as the mean ± standard deviation (SD).
[a]Permeability surface area product on tissue membranes (PS_{muscle}, PS_{skin}, and $PS_{adipose}$) determined in rats were multiplied by a common scaling factor (SF_{PS}). See detail in Methods. [b]*In silico* K_p values in the muscle, skin, and adipose tissues were multiplied by a common scaling factor (SF_{Kp}). See detail in Methods.

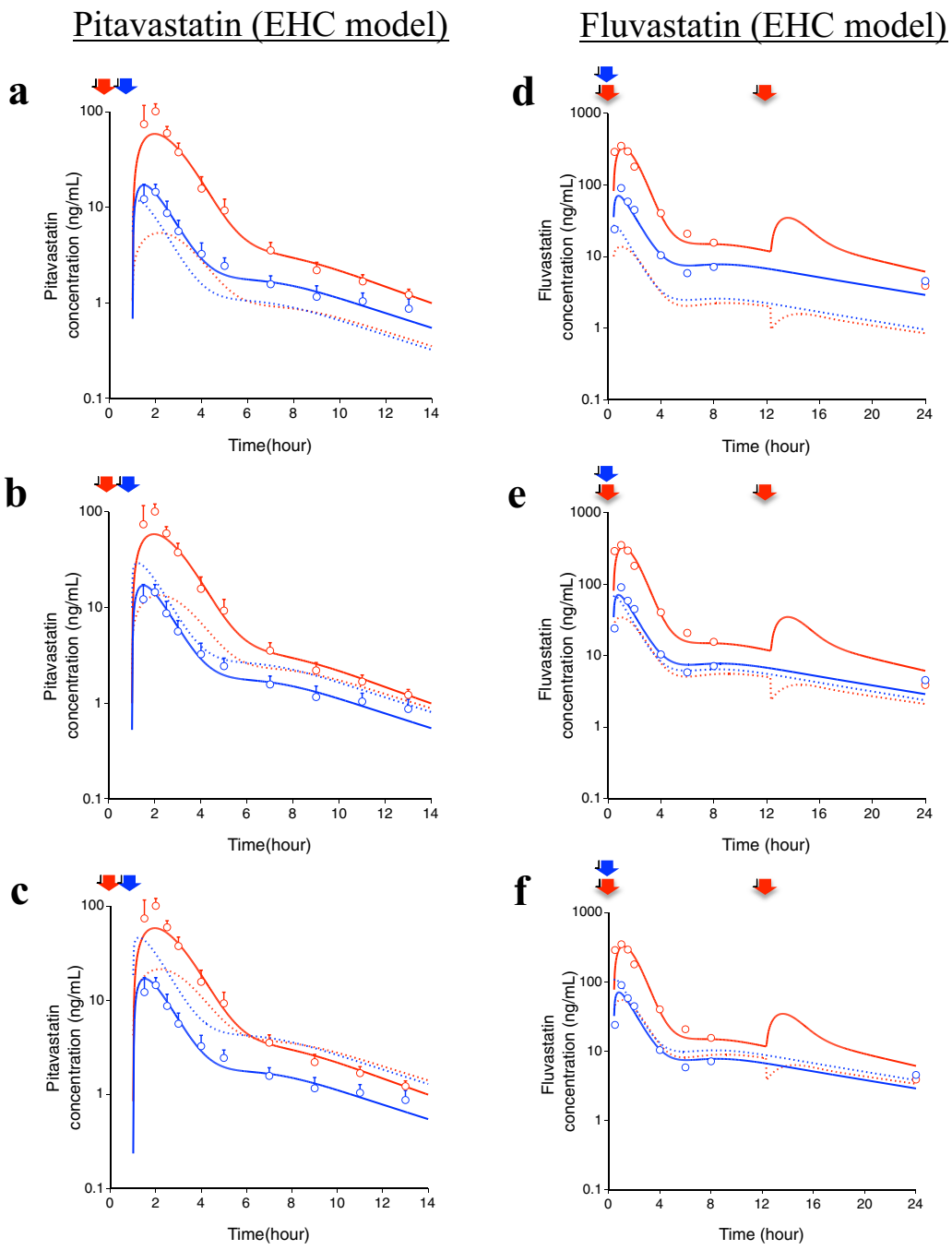

Figure 4 Fitted blood and liver concentration–time profiles of PTV and FLV (EHC models) after the simultaneous optimization of model parameters to explain PK data under both control and DDI (with CsA) conditions using R_{dif} values determined by *in vitro* experiments. The blue and red solid lines represent fitted blood concentration–time profiles of orally administered PTV/FLV under control and DDI conditions, respectively, after parameter optimization in the PBPK model. The blue and red dotted lines represent simulated intrahepatic concentration–time profiles under control and DDI conditions, respectively (the first hepatocytes compartment in **Figure 2**). The circles represent reported concentration–time profiles. **a–c:** Fitting results of PTV. β (= $CL_{int,all}/PS_{inf}$) values were set as 0.8 **(a)**, 0.5 **(b)**, and 0.2 **(c)**. **d–f:** Fitting results of FLV. β values were set as 0.8 **(d)**, 0.5 **(e)**, and 0.2 **(f)**. The blue and red arrows show the timing of the oral administration of statins and CsA, respectively. Optimized parameters are described in **Table 2B** (PTV) and **2C** (FLV).

Simulation of the blood concentration–time profiles of statins considering the inhibition of transporter-mediated biliary excretion by CsA, in addition to the inhibition of hepatic OATPs

PTV and FLV are known substrates of the breast cancer resistance protein (BCRP) and multidrug resistance-associated protein 2 (MRP2).[25,26] Because CsA is an inhibitor of BCRP and MRP2,[5] the inhibition of these biliary excretion transporters may increase the magnitude of DDIs. Considering the inhibition of biliary excretion in addition to the inhibition of hepatic uptake, blood concentration–time profiles of PTV and FLV under DDI conditions were simulated using *in vitro* $K_{i,u}$ values against BCRP

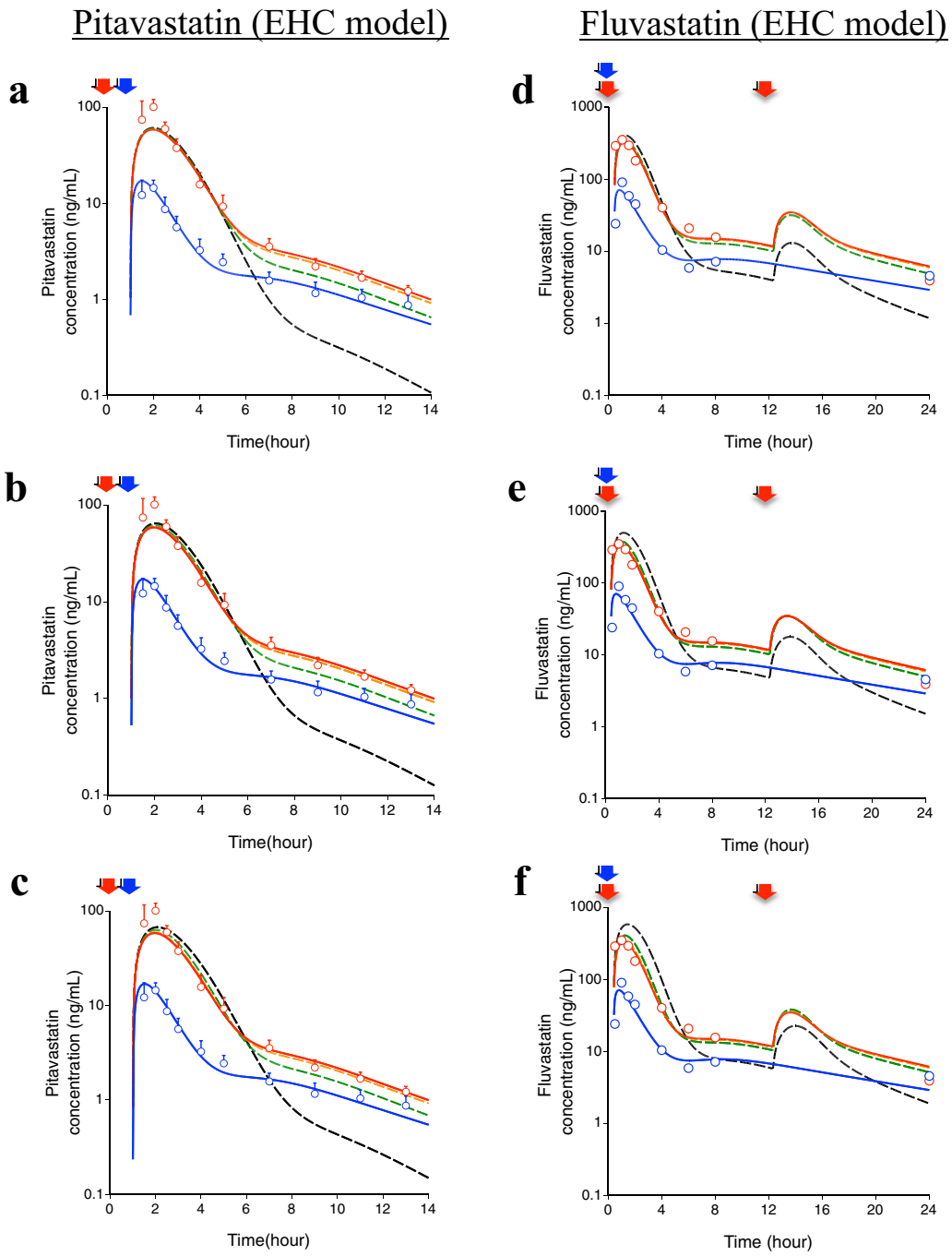

Figure 5 Simulated blood concentration–time profiles of PTV and FLV considering the inhibition of transporter-mediated biliary excretion by CsA, in addition to the inhibition of OATPs-mediated uptake. The solid lines represent fitted blood concentration–time profiles of orally administered statins (PTV/FLV) under control (blue) and DDI conditions (red) considering the inhibition of OATPs-mediated uptake by CsA. The broken lines represent simulated blood concentration–time profiles under DDI conditions considering not only the inhibition of the uptake but also the inhibition of the biliary excretion with reported *in vitro* $K_{i,u}$ = 9.3 μM for MRP2 (orange), $K_{i,u}$ = 1.5 μM for BCRP (green), and hypothetical $K_{i,u}$ = 0.1 μM (black). **a–c:** Simulated results of PTV. β (= $CL_{int,all}/PS_{inf}$) values were set as 0.8 **(a)**, 0.5 **(b)**, and 0.2 **(c)**. **d–f:** Simulated results of FLV. β values were set as 0.8 **(d)**, 0.5 **(e)**, and 0.2 **(f)**. The blue and red arrows show the timing of oral administration of statins and CsA, respectively.

(1.5 μM) or MRP2 (9.3 μM)[5] in addition to the fitted $K_{i,u}$ values against hepatic OATPs (**Figure 5**). As a result, the inhibition of BCRP or MRP2 affected slightly the blood concentration–time profiles of PTV and FLV. The use of a hypothetical $K_{i,u}$ value (0.1 μM) of CsA for biliary excretion process that might cause a strong inhibition of biliary efflux transporters in the simulation led to changes in the blood concentration–time profiles that were caused mainly by the decreased EHC. In addition, the incorporation of the inhibition of biliary efflux transporters alone into the PBPK models did not explain the observed

concentration–time profiles of PTV and FLV in the presence of CsA (data not shown).

DISCUSSION

In this study we aimed to propose a framework for parameter estimation in PBPK model-based analysis of DDIs involving hepatic transporters using *in vivo* information.

The hepatic elimination of statins is comprised of uptake and efflux across the sinusoidal membrane, metabolism, and canalicular efflux into the bile. To aid preparation of the initial parameter of each intrinsic clearance, hybrid parameters (R_{dif}, β, γ, and f_{bile}) were introduced (**Supplemental Text**). Regardless of the fixed β values (0.8, 0.5, and 0.2), similar fitting results were obtained in each case, indicating that it is impossible to optimize β values merely via fitting to the blood concentration data. Conversely, the f_{bile} values of statins were optimized in the analyses: the optimized f_{bile} value for PTV was 0.33 (**Table 2B**), lower than the initial values derived from rat *in vivo* data (**Table 1B**).[27] There might be interspecies differences in biliary excretion and/or metabolism. In contrast, the optimized f_{bile} value for FLV was 0.65 (**Table 2C**) that was rather higher than the initial values from rat data (**Table 1C**),[28] whereas FLV is a well-known substrate for CYP2C9,[29] and its systemic exposure is influenced by CYP2C9 polymorphisms.[30]

Intrahepatic concentrations varied depending on the three β value settings (**Figure 4**). It is essential to predict intrahepatic concentrations of drugs from the perspective of pharmacodynamics/toxicodynamics. The simultaneous fitting of blood/liver/bile concentration–time profiles using nonmetabolized positron emission tomography probes[31,32] might help determine the β values of the probes *in vivo*. In addition, *in vitro* experiments using sandwich-cultured human hepatocytes in which the uptake, efflux, and biliary excretion processes are maintained,[33] whereas metabolisms are not necessarily maintained depending on culturing days,[34] might be useful to construct an IVIVE method of β values. In combination with the evaluation of metabolisms using human liver microsomes or suspended hepatocytes, further top-down and bottom-up analyses should be conducted to increase the accuracy of the prediction of DDIs involving clinically used drugs.

Similar *in vivo* $K_{i,u}$ values of CsA to account for DDI were obtained in this study, regardless of the substrates and initial β values (**Table 2B,C**). Preincubation with CsA *in vitro* potentiates its inhibitory effect on OATP1B1.[7] Amundsen *et al.* reported that $K_{i,u}$ values of CsA against the OATP1B1-mediated transport of atorvastatin were 0.014 and 0.31 μM with or without preincubation, respectively[8]; in another report, $K_{i,u}$ values against five substrates were 0.014–0.080 (geometric mean: 0.0288) and 0.062–0.28 (geometric mean: 0.16) μM with CsA-preincubation and coincubation, respectively. Collectively, *in vitro* $K_{i,u}$ values obtained with CsA-preincubation were similar among OATP substrates and close to the *in vivo* $K_{i,u}$ values obtained in this study. A complex CsA-mediated inhibitory mechanism may be present, which was not assumed in this study, such as trans-inhibition or the inhibition by metabolites of CsA, or AM1,[35] which is also a potent inhibitor of OATP1B1/1B3 *in vitro*. However, the inclusion of inhibition by AM1 resulted in a minor increase in the predicted maximal reduction of OATP1B1/1B3 activity in the PBPK model for the prediction of DDIs between repaglinide and CsA.[35]

To support the effectiveness of our parameter-optimization method in quantitative analysis of the pharmacokinetics of drugs using a PBPK model, and furthermore, DDIs, connecting each PBPK model with drug interaction mechanism, two additional DDI cases with another well-established *in vivo* OATP inhibitor, RIF, were also analyzed (**Suppl. Figs. 3, 4**). Optimized $K_{i,u}$ values for RIF were similar regardless of the substrates (PTV and PRV) and initial β values (**Suppl. Table 3E,F**) although they were somewhat smaller than the reported *in vitro* K_i values against OATP1B1, 0.65-1.1 (geometric mean: 0.92) μM.[36] Namely, once PBPK models are established for substrates and inhibitors, they would help preevaluation of DDI risks of drug combinations that have never been evaluated clinically.

Model-based simulations have been conducted using kinetic parameters extrapolated from *in vitro* parameters assuming the rate-determining process in overall hepatic elimination.[14] Our top-down approach arouses attention in assuming uptake-limited hepatic elimination in the model-based simulations because the β value could not be optimized uniquely even though the time profiles were taken into consideration. However, this approach could help to gain better understanding of the pharmacokinetics of statins (for instance, significant contribution of EHC), although the fact that fitted blood concentration–time curves could not reproduce observed data perfectly as shown in PTV vs. RIF cases (see **Supplemental Text**) indicates room for improvement of the model or parameter estimation. Integration of other clinical data, DDI, and pharmacogenomics studies of drug transporters and metabolizing enzymes, using our model would improve the model and parameter sets.

Several genetic polymorphisms of BCRP and MRP2 affect intestinal drug absorption.[37] Therefore, the inhibition of these efflux transporters by CsA during the absorption process may increase systemic exposure if the F_aF_g of the drug is sufficiently small to be increased by their inhibition. Regarding the PK properties of PTV and FLV, the F_aF_g calculated from the PK data in humans after i.v. and p.o. administration was close to 1, and the effect of CsA on the absorption process should be negligible. It may be necessary to consider the effect of CsA on intestinal absorption, as well as the hepatic elimination of other statins with a relatively small F_aF_g such as rosuvastatin: its F_aF_g is 0.46–0.78[13] and the AUC was significantly increased in subjects with the c.421C>A variant of the BCRP-encoding *ABCG2* gene,[38] suggesting that intestinal and hepatic BCRP might contribute to the clinically observed DDI between rosuvastatin and CsA.[6,39]

In conclusion, the present study proposed a method to analyze *in vivo* PBPK parameters that reproduced adequately the profiles of DDIs between statins and CsA/RIF caused by the inhibition of hepatic OATPs. As β values were not determined just by fitting to the blood concentration–time profiles in this study, it is essential to evaluate β values of positron emission tomography (PET) probes by performing *in vivo* and *in vitro* studies. The accumulation of such analyses to improve IVIVE methods based on both top-down and bottom-up approaches is needed to

establish a methodology for the prediction of complex DDIs involving multiple processes, such as hepatic uptake, biliary excretion, and metabolism.

METHODS

Development of the parameter-optimization method (PTV/FLV vs. CsA)

Construction of the PBPK model. A method to optimize *in vivo* parameters that can explain DDIs caused by the inhibition of hepatic OATPs was developed using PTV/FLV vs. CsA cases (**Figure 1**), which was then tested using PTV/PRV vs. RIF cases (see **Supplemental Text**).

First, the structures of PBPK models were constructed to describe the blood concentration–time profiles of PTV, FLV, and CsA depending on their PK properties (**Figure 2**). In the case of statins, the liver was divided into five units of extrahepatic and hepatocellular compartments that were connected by hepatic blood flow in tandem (5-liver model), which mimics the realistic hepatic disposition based on the dispersion model.[40] In the liver compartments, PS_{act}, $PS_{dif,inf}$, $PS_{dif,eff}$, $CL_{int,bile}$, and $CL_{int,met}$ (all nomenclatures are shown in the **Supplemental Text**) were incorporated, assuming that 1) hepatic-uptake intrinsic clearance is equal to the sum of PS_{act} and $PS_{dif,inf}$, and 2) efflux clearance from the hepatocytes to the blood is equal to $PS_{dif,eff}$. Then, $CL_{int,all}$ can be determined as described below[41]:

$$f_B CL_{int,all} = f_B (PS_{act} + PS_{dif,inf}) \cdot \frac{f_H CL_{int,met} + f_H CL_{int,bile}}{f_H PS_{dif,eff} + f_H CL_{int,met} + f_H CL_{int,bile}} \quad (1)$$

The PBPK models of statins also included compartments for muscle, skin, and adipose tissue, as lipophilic drugs tend to be distributed to these tissues and their contribution to the distribution volume is not always negligible. In addition, because enterohepatic circulation (EHC) of these statins was reported in rats,[27,28] three empirical transit compartments between compartments for hepatocytes and the intestine were incorporated in the models, to describe the delay in EHC processes.

In the case of CsA, as a rapid equilibrium distribution in the liver could be assumed according to a previous report,[42] compartments for extrahepatic tissues and hepatocytes in each unit are unified into a single liver compartment. Based on a previous report indicating the slow distribution of CsA to the tissues,[20] PS_{muscle}, PS_{skin}, and $PS_{adipose}$ were incorporated in the PBPK model. The fractions of tissue cell volume in the muscle (0.854), skin (0.679), and adipose tissue (0.855) were set according to the same report.[42]

The utility and the limit of applying these PBPK models for prospective prediction are described in the **Supplemental Text**.

Setting of parameters in the PBPK models. Basic physiological and pharmacokinetic parameters were collected from previous reports,[43–47] as shown in **Supplemental Table 1A,B**. In addition to $CL_{int,all}$, four hybrid parameters (R_{dif}, β, γ, and f_{bile}) were defined as described in Eqs. 2, 3, 4, and 5, respectively (see detail in the **Supplemental Text**).

$$R_{dif} = \frac{PS_{dif,inf}}{PS_{act}} \quad (2)$$

$$\beta = \frac{f_H CL_{int,met} + f_H CL_{int,bile}}{f_H PS_{dif,eff} + f_H CL_{int,met} + f_H CL_{int,bile}} \quad (3)$$

$$\gamma = \frac{PS_{dif,inf}}{PS_{dif,eff}} \quad (4)$$

$$f_{bile} = \frac{CL_{int,bile}}{CL_{int,met} + CL_{int,bile}} \quad (5)$$

Thus, PS_{act}, $PS_{dif,inf}$, $PS_{dif,eff}$, $CL_{int,met}$, and $CL_{int,bile}$ can be calculated from $CL_{int,all}$ and these four hybrid parameters.

The R_{dif} values of statins were calculated according to Eqs. 2 and 6[24]:

$$PS_{act} + PS_{dif,inf} = \frac{V_{max}}{K_m} + PS_{dif,inf} \quad (6)$$

where V_{max}/K_m and $PS_{dif,inf}$ were determined via the *in vitro* uptake studies using cryopreserved human hepatocytes described in the **Supplemental Text**. Three different fixed β values (0.8, 0.5, and 0.2) were used in the PBPK model of each statin, because it was difficult to optimize all other parameters without setting the β values. These fixed β values indicate different conditions of the major rate-determining processes in the overall hepatic intrinsic clearance[41]: in Eq. 1, when CL_{int} (= $CL_{int,bile}$ + $CL_{int,met}$) is significantly greater than $PS_{dif,eff}$ (high β), $CL_{int,all}$ can be approximated to PS_{inf} (= PS_{act} + $PS_{dif,inf}$), and it does not depend on PS_{eff} and CL_{int}. By contrast, when CL_{int} is negligibly lower than $PS_{dif,eff}$ (low β), $CL_{int,all}$ can be affected by not only uptake, but also metabolism and biliary excretion. Subsequently, γ values were determined using the following three parameters: 1) the ratio of the membrane permeation clearance by passive diffusion of an ionized form of the drug to that of its unionized form, which can be obtained from *in vitro* experiments that examine pH-dependent membrane permeability[48]; 2) the concentration ratio of an ionized form of the drug to its unionized form, derived from the Henderson–Hasselbalch equation (intracellular pH = 7.2, extracellular pH = 7.4); and 3) the membrane potential estimated from the Nernst equation. The calculated γ values were 0.244 for PTV and 0.243 for FLV, which were fixed in the parameter-optimization step (**Table 2**).

Using two-compartmental analyses, the initial values of k_a and T_{lag} were estimated simultaneously, to fit the calculated results to the reported concentration–time profiles after single oral administrations of PTV and FLV:

$$C(t) = -A \cdot \exp[-K_a(t - T_{lag})] + B \cdot \exp[-K_1(t - T_{lag})] + D \cdot \exp[-K_2(t - T_{lag})] \quad (7)$$

In the case of CsA, the k_a and T_{lag} values reported previously[42] were used as initial parameters.

The $V_{central}$ was fixed to the blood volume (0.075 L/kg).[44] The F_aF_g values of statins and CsA shown in **Supplemental Table 1B** were calculated based on Eq. 8:

$$F_a F_g = \frac{F}{F_h} = F \cdot \frac{Q_H}{Q_H - (CL_{tot} - CL_R)} \quad (8)$$

It was assumed that the liver was the only organ of statins/CsA elimination because their CL_R values were nearly equal to zero according to previous reports.[5,42] The F_aF_g values of PTV and FLV were calculated according to a previous report.[5] Regarding CsA, the F_aF_g of Sandimmune was first calculated using the PK data after i.v. and p.o. administration of the drug.[45] Then, the F_aF_g of Neoral was estimated by comparing the AUCs of the two formulations described in a previous report.[46]

The initial $f_B CL_{int,all}$ values of statins were calculated using Eqs. 9 and 10 (non-EHC model) or Eqs. 9 and 11 (EHC model), which were derived from equations given in the **Supplemental Text** at the steady-state condition[40]:

$$f_B CL_{\mathrm{int},all} = 5 \cdot Q_H \cdot \left[\left(\frac{1}{F\prime_h} \right)^{\frac{1}{5}} - 1 \right] \quad (9)$$

$$\frac{F_a F_{g,BA} Dose_{DDI}}{AUC_{DDI}} = \frac{1}{(F\prime_h)^5} \cdot (Q_H + CL_{R,DDI}) - Q_H \quad (10)$$

$$\frac{F_a F_{g,BA} Dose_{DDI}}{AUC_{DDI}} = \left[1 + (1 - f_{bile} F_a F_{g,BA}) \left[\frac{1}{(F\prime_h)^5} - 1 \right] \right] \cdot (Q_H + CL_{R,DDI}) - Q_H \quad (11)$$

where F'_h is the hepatic availability in the 5-liver model[40] and f_{bile} is a parameter that determines the ratio of biliary excretion and metabolism in the EHC model, as shown in Eq. 5. The initial values of f_{bile} of statins were calculated using Eq. 12 and the PK data in the bile duct-cannulated rats.[27,28]

$$f_{bile,rat} = \frac{\%dose\_excreted\_to\_bile\_as\_unchanged\_form}{100 - \%\,dose\_excreted\_to\_urine\_as\_unchanged\_form} \quad (12)$$

Based on the reported *in silico* methodology[49] that uses clogP and pK_a described in SciFinder Scholar (Chemical Abstracts Service, Columbus, OH), $K_{p,muscle}$, $K_{p,skin}$, and $K_{p,adipose}$ were calculated (**Supplemental Table 1B**). In the case of CsA, the *in silico* K_p values in the muscle, skin, and adipose tissue were multiplied by a common scaling factor (SF_{Kp}) (**Table 1A**), which was optimized in the fitting step (**Table 2A**). In addition, membrane-permeability processes were taken into account for muscle, skin, and adipose tissue, according to a previous report[42]; PS_{muscle}, PS_{skin}, and $PS_{adipose}$ determined in rats were multiplied by a common scaling factor (SF_{PS}) (**Table 1A**), which was also optimized by fitting (**Table 2A**). The $K_{p,liver}$ in rats was set as the initial parameter in the PBPK model.[42] The $f_H CL_{int}$ of CsA was determined based on the clearance concept using the PK data after i.v. administration of the drug.[45]

The initial value for the $K_{i,total}$ of CsA on the PS_{act} of statins was calculated using the following equation[5]:

$$AUCR = 1 + \frac{I_{max}}{K_{i,total}} \quad (13)$$

where AUCR represents the AUC ratio of each statin reported in the clinical DDI reports[16,17] and I_{max} represents the maximum concentration of CsA in the liver extracellular space calculated by dividing the simulated liver maximum concentration in each DDI case by $K_{p,liver}$. The $K_{i,u}$ was calculated by multiplying $K_{i,total}$ by f_B.

The criteria for adopting initial and fixed values of parameters are summarized in **Supplemental Text**.

Parameter optimization by nonlinear least-squares fitting. The PK parameters of PTV, FLV, and CsA in the PBPK models were optimized by fitting to their blood concentration–time profiles.[16,17,20] In the cases of PTV and FLV, blood concentrations were calculated using the plasma concentrations provided in previous reports and the R_B values described in **Supplemental Table 1B**. The nonlinear least-squares fitting software Napp, v. 2.31,[50] was used in all the optimization and simulation processes applied in this study. The weight for the nonlinear least-squares calculation was set at one (the square root of the value). The WSS and Akaike's Information Criterion (AIC), as shown in Eqs. 14 and 15, respectively, were used for the evaluation of fitting results.

$$WSS = \sum_{i=1}^{n} \frac{(y_i - y'_i)^2}{y_i} \quad y_i : i\text{th observed value}, y'_i : i\text{th predicted value} \quad (14)$$

$$AIC = n \ln WSS + 2m \quad (15)$$

Additional Supporting Information may be found in the online version of this article.

ACKNOWLEDGMENTS

The first two authors contributed equally to this work. The study was financially supported by Grant-in-Aid for Scientific Research (S) and the Scientific Research on Innovative Areas HD-Physiology from the Ministry of Education, Culture, Sports, Sciences, and Technology in Japan (Grants 24229002; 23136101).

CONFLICT OF INTEREST/DISCLOSURE

The authors declare no conflicts of interest.

AUTHOR CONTRIBUTIONS

T.Y., K.Y., K.M., H.K., and Y.S. wrote the article. T.Y., K.Y., K.M., H.K., and Y.S. designed the research; T.Y., K.Y., N.K., T.N., R.A., K.T., K.M., and Y.S. performed the research; T.Y., K.Y., K.M., and Y.S. analyzed the data.

1. Bruno-Joyce, J., Dugas, J.M. & MacCausland, O.E. Cerivastatin and gemfibrozil-associated rhabdomyolysis. *Ann. Pharmacother.* **35**, 1016–1019 (2001).
2. Roca, B., Calvo, B. & Monferrer, R. Severe rhabdomyolysis and cerivastatin-gemfibrozil combination therapy. *Ann. Pharmacother.* **36**, 730–731 (2002).
3. Shitara, Y., Hirano, M., Sato, H. & Sugiyama, Y. Gemfibrozil and its glucuronide inhibit the organic anion transporting polypeptide 2 (OATP2/OATP1B1:SLC21A6)-mediated hepatic uptake and CYP2C8-mediated metabolism of cerivastatin: analysis of the mechanism of the clinically relevant drug-drug interaction between cerivastatin and gemfibrozil. *J. Pharmacol. Exp. Ther.* **311**, 228–236 (2004).
4. Shitara, Y. & Sugiyama, Y. Pharmacokinetic and pharmacodynamic alterations of 3-hydroxy-3-methylglutaryl coenzyme A (HMG-CoA) reductase inhibitors: drug-drug interactions and interindividual differences in transporter and metabolic enzyme functions. *Pharmacol. Ther.* **112**, 71–105 (2006).
5. Yoshida, K., Maeda, K. & Sugiyama, Y. Transporter-mediated drug-drug interactions involving OATP substrates: predictions based on in vitro inhibition studies. *Clin. Pharmacol. Ther.* **91**, 1053–1064 (2012).
6. Elsby, R., Hilgendorf, C. & Fenner, K. Understanding the critical disposition pathways of statins to assess drug-drug interaction risk during drug development: it's not just about OATP1B1. *Clin. Pharmacol. Ther.* **92**, 584–598 (2012).
7. Shitara, Y. *et al*. Long-lasting inhibitory effects of cyclosporin A, but not tacrolimus, on OATP1B1- and OATP1B3-mediated uptake. *Drug Metab. Pharmacokinet.* **27**, 368–378 (2012).
8. Amundsen, R., Christensen, H., Zabihyan, B. & Asberg, A. Cyclosporine A, but not tacrolimus, shows relevant inhibition of organic anion-transporting protein 1B1-mediated transport of atorvastatin. *Drug Metab. Dispos.* **38**, 1499–1504 (2010).
9. Kato, M. *et al*. The quantitative prediction of CYP-mediated drug interaction by physiologically based pharmacokinetic modeling. *Pharmaceut. Res.* **25**, 1891–1901 (2008).
10. Fahmi, O.A. *et al*. Comparison of different algorithms for predicting clinical drug-drug interactions, based on the use of CYP3A4 in vitro

data: predictions of compounds as precipitants of interaction. *Drug Metab. Dispos.* **37**, 1658–1666 (2009).
11. Morrissey, K.M. *et al*. The UCSF-FDA TransPortal: a public drug transporter database. *Clin. Pharmacol. Ther.* **92**, 545–546 (2012).
12. Varma, M.V. *et al*. Physiologically based modeling of pravastatin transporter-mediated hepatobiliary disposition and drug-drug interactions. *Pharmaceut. Res.* **29**, 2860–2873 (2012).
13. Jamei, M. *et al*. A mechanistic framework for in vitro-in vivo extrapolation of liver membrane transporters: prediction of drug-drug interaction between rosuvastatin and cyclosporine. *Clin. Pharmacokinet.* **53**, 73–87 (2014).
14. Li, R., Barton, H.A. & Varma, M.V. Prediction of pharmacokinetics and drug-drug interactions when hepatic transporters are involved. *Clin. Pharmacokinet.* **53**, 659–678 (2014).
15. Yoshida, K., Maeda, K. & Sugiyama, Y. Hepatic and intestinal drug transporters: prediction of pharmacokinetic effects caused by drug-drug interactions and genetic polymorphisms. *Annu. Rev. Pharmacol. Toxicol.* **53**, 581–612 (2013).
16. Hasunuma, T. *et al*. The drug-drug Interactions of pitavastatin (NK-104), a novel HMG-CoA reductase Inhibitor and cyclosporine. *J. Clin. Ther. Med.* **19**, 381–389 (2003).
17. Park, J.W. *et al*. Pharmacokinetics and pharmacodynamics of fluvastatin in heart transplant recipients taking cyclosporine A. *J. Cardiovasc. Pharmacol. Ther.* **6**, 351–361 (2001).
18. Chen, Y. *et al*. Effect of a single-dose rifampin on the pharmacokinetics of pitavastatin in healthy volunteers. *Eur. J. Clin. Pharmacol.* **69**, 1933–1938 (2013).
19. Maeda, K. *et al*. Identification of the rate-determining process in the hepatic clearance of atorvastatin in a clinical cassette microdosing study. *Clin. Pharmacol. Ther.* **90**, 575–581 (2011).
20. Mueller, E.A., Kovarik, J.M., van Bree, J.B., Lison, A.E. & Kutz, K. Pharmacokinetics and tolerability of a microemulsion formulation of cyclosporine in renal allograft recipients—a concentration-controlled comparison with the commercial formulation. *Transplantation* **57**, 1178–1182 (1994).
21. Kimoto, E. *et al*. Characterization of organic anion transporting polypeptide (OATP) expression and its functional contribution to the uptake of substrates in human hepatocytes. *Mol. Pharmaceut.* **9**, 3535–3542 (2012).
22. Menochet, K., Kenworthy, K.E., Houston, J.B. & Galetin, A. Use of mechanistic modeling to assess interindividual variability and interspecies differences in active uptake in human and rat hepatocytes. *Drug Metab. Dispos.* **40**, 1744–1756 (2012).
23. Nordell, P., Winiwarter, S. & Hilgendorf, C. Resolving the distribution-metabolism interplay of eight OATP substrates in the standard clearance assay with suspended human cryopreserved hepatocytes. *Mol. Pharmaceut.* **10**, 4443–4451 (2013).
24. Jones, H.M. *et al*. Mechanistic pharmacokinetic modeling for the prediction of transporter-mediated disposition in humans from sandwich culture human hepatocyte data. *Drug Metab. Dispos.* **40**, 1007–1017 (2012).
25. Li, J. *et al*. Use of transporter knockdown Caco-2 cells to investigate the in vitro efflux of statin drugs. *Drug Metab. Dispos.* **39**, 1196–1202 (2011).
26. Hirano, M. *et al*. Involvement of BCRP (ABCG2) in the biliary excretion of pitavastatin. *Mol. Pharmacol.* **68**, 800–807 (2005).
27. Fujino, H., Yamada, I., Shimada, S. & Kojima, J. Metabolic fate of pitavastatin, a new inhibitor of HMG-CoA reductase—effect of cMOAT deficiency on hepatobiliary excretion in rats and of mdr1a/b gene disruption on tissue distribution in mice. *Drug Metab. Pharmacokinet.* **17**, 449–456 (2002).
28. Tse, F.L., Smith, H.T., Ballard, F.H. & Nicoletti, J. Disposition of fluvastatin, an inhibitor of HMG-COA reductase, in mouse, rat, dog, and monkey. *Biopharm. Drug Dispos.* **11**, 519–531 (1990).
29. Scripture, C.D. & Pieper, J.A. Clinical pharmacokinetics of fluvastatin. *Clin. Pharmacokinet.* **40**, 263–281 (2001).
30. Kirchheiner, J. *et al*. Influence of CYP2C9 polymorphisms on the pharmacokinetics and cholesterol-lowering activity of (-)-3S,5R-fluvastatin and (+)-3R,5S-fluvastatin in healthy volunteers. *Clin. Pharmacol. Ther.* **74**, 186–194 (2003).
31. Takashima, T. *et al*. The involvement of organic anion transporting polypeptide in the hepatic uptake of telmisartan in rats: PET studies with [(1)(1)C]telmisartan. *Mol. Pharmaceut.* **8**, 1789–1798 (2011).
32. Shingaki, T. *et al*. Evaluation of Oatp and Mrp2 activities in hepatobiliary excretion using newly developed positron emission tomography tracer [11C]dehydropravastatin in rats. *J. Pharmacol. Exp. Ther.* **347**, 193–202 (2013).
33. Liu, X. *et al*. Partial maintenance of taurocholate uptake by adult rat hepatocytes cultured in a collagen sandwich configuration. *Pharmaceut. Res.* **15**, 1533–1539 (1998).
34. Kimoto, E. *et al*. Differential modulation of cytochrome P450 activity and the effect of 1-aminobenzotriazole on hepatic transport in sandwich-cultured human hepatocytes. *Drug Metab. Dispos.* **40**, 407–411 (2012).
35. Gertz, M. *et al*. Cyclosporine inhibition of hepatic and intestinal CYP3A4, uptake and efflux transporters: application of PBPK modeling in the assessment of drug-drug interaction potential. *Pharmaceut. Res.* **30**, 761–780 (2013).
36. Izumi, S. *et al*. Investigation of the impact of substrate selection on in vitro organic anion transporting polypeptide 1B1 inhibition profiles for the prediction of drug-drug interactions. *Drug Metab. Dispos.* **43**, 235–247 (2015).
37. Ieiri, I., Higuchi, S. & Sugiyama, Y. Genetic polymorphisms of uptake (OATP1B1, 1B3) and efflux (MRP2, BCRP) transporters: implications for inter-individual differences in the pharmacokinetics and pharmacodynamics of statins and other clinically relevant drugs. *Expert Opin. Drug Metabol. Toxicol.* **5**, 703–729 (2009).
38. Zhang, W. *et al*. Role of BCRP 421C>A polymorphism on rosuvastatin pharmacokinetics in healthy Chinese males. *Clin. Chim. Acta* **373**, 99–103 (2006).
39. Simonson, S.G. *et al*. Rosuvastatin pharmacokinetics in heart transplant recipients administered an antirejection regimen including cyclosporine. *Clin. Pharmacol. Ther.* **76**, 167–177 (2004).
40. Watanabe, T., Kusuhara, H., Maeda, K., Shitara, Y. & Sugiyama, Y. Physiologically based pharmacokinetic modeling to predict transporter-mediated clearance and distribution of pravastatin in humans. *J. Pharmacol. Exp. Ther.* **328**, 652–662 (2009).
41. Watanabe, T., Kusuhara, H. & Sugiyama, Y. Application of physiologically based pharmacokinetic modeling and clearance concept to drugs showing transporter-mediated distribution and clearance in humans. *J. Pharmacokinet. Pharmacodyn.* **37**, 575–590 (2010).
42. Kawai, R., Mathew, D., Tanaka, C. & Rowland, M. Physiologically based pharmacokinetics of cyclosporine A: extension to tissue distribution kinetics in rats and scale-up to human. *J. Pharmacol. Exp. Ther.* **287**, 457–468 (1998).
43. Watanabe, T. *et al*. Prediction of the overall renal tubular secretion and hepatic clearance of anionic drugs and a renal drug-drug interaction involving organic anion transporter 3 in humans by in vitro uptake experiments. *Drug Metab. Dispos.* **39**, 1031–1038 (2011).
44. Davies, B. & Morris, T. Physiological parameters in laboratory animals and humans. *Pharmaceut. Res.* **10**, 1093–1095 (1993).
45. Ducharme, M.P., Warbasse, L.H. & Edwards, D.J. Disposition of intravenous and oral cyclosporine after administration with grapefruit juice. *Clin. Pharmacol. Ther.* **57**, 485–491 (1995).
46. Mueller, E.A. *et al*. Influence of a fat-rich meal on the pharmacokinetics of a new oral formulation of cyclosporine in a crossover comparison with the market formulation. *Pharmaceut. Res.* **11**, 151–155 (1994).
47. Lemaire, M. & Tillement, J.P. Role of lipoproteins and erythrocytes in the in vitro binding and distribution of cyclosporin A in the blood. *J. Pharm. Pharmacol.* **34**, 715–718 (1982).
48. Varma, M.V. *et al*. pH-sensitive interaction of HMG-CoA reductase inhibitors (statins) with organic anion transporting polypeptide 2B1. *Mol. Pharmaceut.* **8**, 1303–1313 (2011).
49. Rodgers, T. & Rowland, M. Physiologically based pharmacokinetic modelling 2: predicting the tissue distribution of acids, very weak bases, neutrals and zwitterions. *J. Pharmaceut. Sci.* **95**, 1238–1257 (2006).
50. Hisaka, A. & Sugiyama, Y. Analysis of nonlinear and nonsteady state hepatic extraction with the dispersion model using the finite difference method. *J. Pharmacokinet. Biopharmaceut.* **26**, 495–519 (1998).